Desalination and Water Treatment
www.deswater.com

doi: 10.5004/dwt.2019.23321

143 (2019) 282–294
March

Magnetic flocculation of anion dyes by a novel composite coagulant

Xiaoyue Chen[a,b], Huaili Zheng[a,b,*], Wenying Xiang[a,b], Yanyan An[a,b], Bincheng Xu[a,b], Chuanliang Zhao[a,b], Shixing Zhang[a,b]

[a]*Key Laboratory of the Three Gorges Reservoir Region's Eco-Environment, State Ministry of Education, Chongqing University, Chongqing 400045, China, Tel/Fax: +86 23 65120827; emails: zhl@cqu.edu.cn (H. Zheng), cxy-sc@qq.com (X. Chen), xwy829@126.com (W. Xiang), 747738515@qq.com (Y. An), 1579505026@qq.com (B. Xu), 1213211435@qq.com (C. Zhao), xiyu998888@163.com (S. Zhang)*
[b]*National Centre for International Research of Low-Carbon and Green Buildings, Chongqing University, Chongqing 400045, China*

Received 8 April 2018; Accepted 22 October 2018

ABSTRACT

A novel nano-magnetic particles–polyferric sulfate composite coagulant (Fe_3O_4–PFS) was firstly produced. In this study, the pre-polymerized ion-based PFS and Fe_3O_4 were combined (Fe_3O_4–PFS) to remove a typical anion dye, Congo Red. Fe_3O_4–PFS with different molar ratio of PFS (30–100 mg/L) to Fe_3O_4 (0–600 mg/L) showed good performance at the studied pH range, especially at pH 7. The removal value increased from 29.5% to 64.8% when 500 mg/L of Fe_3O_4 was added into 30 mg/L of PFS. The structure and morphology property of the aggregated flocs induced by the composite coagulant were analyzed through instrumental analyses such as Fourier-transform infrared spectroscopy, X-ray diffractometer, scanning electron microscope, a physical property measurement system equipped with vibrating-sample magnetometer, and optical microscope. To study the influence of Fe_3O_4, fractal dimension (D_f) of flocs was investigated by employing image analysis. Finally, the effects and interactions of various factors on the treatment efficiency were studied by response surface methodology coupled with Box–Behnken design. The results showed that the Fe_3O_4–PFS–CR flocs induced by some local charge interactions and cheating were successfully formed. The flocs of Fe_3O_4–PFS–CR were lager, compacter, and denser. The surface of it exhibits rougher and more porous. This coagulant significantly decreased the dosage of inorganic coagulant, the flocculation time, and exhibited slighter pH dependence compared with PFS. The respective tests confirmed that the predominant coagulation mechanism of Fe_3O_4–PFS is the adsorbing-bridging. The method can greatly improve the color removal value. The novel method was highly efficient and environmentally feasible, which it seemed to hold considerable potential in the purification processes of real wastewater.

Keywords: Congo Red; Fe_3O_4; Polyferric sulfate; Magnetic flocculation; Water treatment

1. Introduction

With the development of the economy, the environmental problems have drawn our attention. Various water treatment processes have been utilized, such as adsorption [1], coagulation–flocculation [2], ion exchange [3], advanced oxidation [4], membrane filtration [5], and biological methods [6]. Among those methods, coagulation–flocculation is one of the widely used processes, which has a long history.

Inorganic metal salts have been widely used for decades as coagulants. It is useful to remove very fine suspended solids, inorganic, and organic dissolved particles [7]. Besides, it is easy to use and affordable. However, its low flocculation efficiency and some severe environmental circumstances limit its application. As reported in many studies, these inorganic metal salts are highly sensitive to pH, temperature, and low-concentration impurities. The pre-hydrolyzed metal

* Corresponding author.

coagulants in some extent improve the performance, but the problem of large volumes of metal hydroxide (toxic) and residual metal concentration (e.g., aluminum) still exists, which has a possible link with pathogenesis of Alzheimer's disease [8].

In recent years, organic synthetic materials have been enjoying a boom. Various organic flocculants have been synthesized. They have different molecular weight, structure (linear or branched), amount of charge, charge type, and composition. These organic flocculants can achieve better flocculation efficiency, form bigger and stronger flocs, which have good settling characteristics and do not affect the pH of the medium. However, its market cost is higher than the inorganic flocculants, and it is lack of biodegradability. In addition, its application may cause health hazards, which generally arise from residual unreacted monomers. All of these characteristics restrain its application.

With the increase demand of environmentally friendly materials to treat wastewater, natural bioflocculants, such as chitosan [9], tannin [10], gums and mucilage [11], sodium alginate [12], and cellulose [13] have attracted wide interests of researchers. They are biodegradable and produce no secondary pollution, but their short shelf life, high cost, and less effectiveness are big challenges.

The continuous increasing needs for more efficient and environmentally friendly flocculants have induced the development of magnetic coagulation. Compared with the traditional coagulants–flocculants methods, magnetic coagulation–flocculation has many unique characteristics. Most of the Fe_3O_4 particles used for magnetic coagulation are prepared by chemical reactions such as co-precipitation, thermal decomposition, metal reduction, and the like. These Fe_3O_4 particles are nearly spherical, have a uniform particle size distribution, and can reach nanometer. In the field of wastewater treatment, there are many studies on the removal of heavy metals and algae using Fe_3O_4 particles [14–19]. In these studies, it was found that Fe_3O_4 particles have a large removal capacity, fast kinetics, and high reactivity for contaminant removal for its extremely small particle size and high surface-area-to-volume ratio. In the meanwhile, Fe_3O_4 particles have one more important property, that is, magnetism, which allows it to use artificial magnetic field to quickly remove contaminants. It not only can improve the removal value but also can be reused by desorbing contaminants, which has greatly expanded its range of applications. Therefore, Fe_3O_4 can be used for protein immobilization, drug controlled release, wastewater treatment, and metal processing. Magnetic coagulation combines flocs with Fe_3O_4. Then by means of magnetic separation, it can realize rapid removal of impurities. The Fe_3O_4 in the sludge can be recycled, and it can achieve a substantial reduction in sludge treatment capacity. Chin et al. [20] synthesized magnetic nanoparticles to remove silica nanoparticles from chemical mechanical polishing (CMP) wastewaters. It was found that silica and magnetite nanoparticles were oppositely charged between pH 2.2 and 6.7. Silica nanoparticles from CMP wastewater were removed by electrostatic attractions under magnetic field, and the sufficient collisions played an important role in the process. The research on harvesting *Chlorella vulgaris* by magnetic flocculation shows that the ζ-potential of composite PACl (polyaluminum chloride)/Fe_3O_4 was increased and thus a better result was achieved under a magnetic field [21]. Nevertheless, magnetic coagulation mechanism is still in its infancy. In some places, magnetic field can achieve good results, but in some other places, it has completely failed. Currently, magnetic flocculation has been applied in the removing of algae [22,23], heavy metals [24,25], and wastewater sludge dewatering [26]. Certain progress has been made in the field of removing phosphate by magnetic flocculation [27]. However, there is almost no report on the removal of soluble dyes by magnetic coagulation.

In this study, polyferric sulfate (PFS) and Fe_3O_4 were combined and used as coagulant, and Congo Red was chosen as a typical anionic dye. The effects of dosage, dosing strategy, and the ratio of PFS to Fe_3O_4 (mg/L) on the dye removal were investigated in the absence of external magnetic field. The structure and morphology of flocs were characterized using Fourier-transform infrared spectroscopy (FTIR), scanning electron microscope (SEM), and the optical microscope. The D_f was studied by image analysis. Moreover, the coagulation mechanism was studied. This study can provide a reference for the further theoretical study of magnetic coagulation.

2. Materials and methods

2.1. Materials

Congo Red was obtained from Tianjin Damao Chemical Reagent Factory (Tianjin, China). NaOH and HCL were supplied by Shandong Chemical Plant (Jinan, Shandong province, China).

All reagents were of analytical grade and used as received without further purification, and tap water was used in the coagulation experiments.

2.2. Preparation of PFS–Fe_3O_4 composite coagulant

Fe_3O_4 (50 nm) and PFS were purchased from Cheng Du Micxy Chemical. Co., Ltd., Chengdu, Sichuan province, China.

The PFS–Fe_3O_4 composite coagulants at different PFS to Fe_3O_4 ratios were subsequently prepared by inserting a pre-determined amount of Fe_3O_4 into water–based PFS stock solution (500 mg/L) under stirring for 2 min to form a uniform and stable solution.

2.3. Magnetic flocculation

A total of 1 g/L stock solution of Congo Red (CR) was prepared by dissolving 1 g CR in 1 L tap water. The chemical structure of CR is shown in Fig. 1.

The experiments were carried out in a jar test apparatus (TA6, Wuhan Hengling Technology Co., Ltd., China). The test suspension was prepared by diluting the stock CR solution

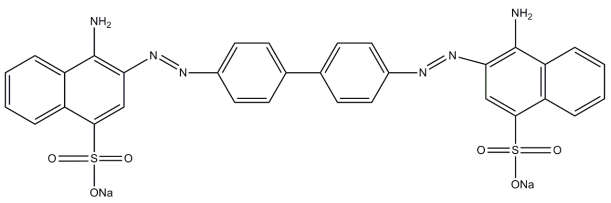

Fig. 1. Structure of CR.

with tap water to obtain the concentration of 100 mg/L. An appropriate amount of coagulant was dosed. Then, the flocculation period (3 min at 250 rpm paddle velocity and 15 min at 80 rpm paddle velocity) and the final sedimentation step (2 min) were applied afterwards. After that, 10 mL sample was collected from 2 cm below the water surface.

Coagulation experiments were conducted at different ratio of composite coagulant Fe_3O_4–PFS. The dosage of PFS and Fe_3O_4 were varied from 0 to 600 mg/L and 30 to 100 mg/L, respectively. To investigate the effect of pH on the removal of CR, the pH of test water was adjusted in the range of 4–10 by adding HCl (1 M, 0.1 M) and NaOH (1 M, 0.1 M) solutions. The dosage of PFS and Fe_3O_4 was fixed at 50 and 200 mg/L, respectively. The measurement of pH was carried out using a pH700 pH meter (Eutech, USA).

There are three dosing strategies to test the mechanism of the coagulation process. That is, PFS+Fe_3O_4 (PFS was dosed first followed by Fe_3O_4), Fe_3O_4+PFS (Fe_3O_4 was dosed first followed by PFS), and PFS–Fe_3O_4. The final concentrations of PFS in all the three strategies were kept the same, that is, 50 mg/L, while the dosage of Fe_3O_4 was varied from 0 to 600 mg/L.

2.4. Analytical methods

Zeta (ζ)-potential measurements were performed on a Zetasizer Nano ZS90 (Malvern Instruments Ltd., Malvern, UK). The concentration of CR was analyzed by a UV–Vis spectrometer by monitoring the absorbance (500 nm) after filtration by of 0.46 μm membrane (mixed cellulose, Navigator). The zeta (ζ) potential of the supernatants was analyzed immediately after flocculation.

The zeta (ζ) potential of Fe_3O_4 particles (0.6 g/L) was investigated using Zetasizer Nano ZS90 (Malvern Instruments Ltd., Malvern, UK). FTIR spectra of the CR, PFS, Fe_3O_4, floc1 (only PFS), and floc2 (PFS and Fe_3O_4) were recorded by an FTIR spectrometer (Nicolet iS5, Nicolet, USA) using KBr pellets. The images of the flocs were investigated by a microscope. The size distribution was measured using a particle size analyzer (Mastersizer 2000, Malvern, UK). X-ray diffraction (XRD) patterns were obtained with XRD (DMAX/2C) using graphite monochromatized Cu Kα radiation (λ = 1.54056 Å). Magnetic properties were performed with a physical property measurement system (PPMS) equipped with vibrating-sample magnetometer (PPMS DynaCool 9, Quantum Design, USA). The surface morphologies of the two different flocs were observed by an SEM-type TESCAN MIRA3 under an acceleration voltage of 10.0 kV.

Leaching of Fe from Fe_3O_4 was measured by inductively coupled plasma-optical emission spectroscopy. 0.1 g of dried Fe_3O_4 is added into 250 mL water at different pH levels in each conical flask.

2.5. Fractal dimension

The method put forward by Chakraborti et al. [28] was applied to calculate the two-dimensional fractal dimension of irregular image. The flocs were shaped on slide glass and recorded by microscope. The image was analyzed by image-pro plus. Fractals, D_f, was calculated according to the following equation:

$$A \propto p^{D_f} \tag{1}$$

where A and p are the projected area and the perimeter of flocs, respectively.

2.6. Response surface methodology coupled with Box–Behnken design (RSM–BBD)

The RSM–BBD was employed for the optimization of the parameters including initial pH value (X_1), coagulant dosage (X_2), the initial concentration (X_3), and ionic strength of KCl (X_4) on the response functions, which are listed in Table S1. The experimental data were analyzed and fitted to a second-order polynomial model using Design Expert 10 to optimize the variables in the coagulation–flocculation process.

$$Y = \beta_0 + \sum_{I=1}^{K} \beta_1 X_i + \sum_{i=1}^{j-1} \sum_{i=1}^{k} \beta_{ij} X_i X_j + \sum_{i=1}^{k} \beta_{ij} X_i^2 \tag{2}$$

where Y is the response for the residual turbidity of surfactant effluent, β_0 is the constant coefficient, β_i is the linear coefficient, β_{ij} is the interaction coefficient, and X_i and X_j refer to variables. These analyses are carried out by virtue of R^2 values, Fisher's F–test, and P-value (probability).

3. Results and discussion

3.1. Properties of Fe_3O_4

Fig. 2 presents the adsorption ability of Fe_3O_4. Prior to any sort of conclusion made by the application of this method, it is more than necessary whether Fe_3O_4 will adsorb CR rather than flocculate. We can see that the CR remained at 100 mg/L after various doses of Fe_3O_4 were added. It can be revealed from Fig. 2 that Fe_3O_4 particles have almost no effect on the removal of the dye. Therefore, in this experiment, the Fe_3O_4 could not remove CR by adsorption. However, in the previous study, it was found that Fe_3O_4 can adsorb the dye on to its surface. It may be due to the different preparation methods that lead to different properties or the too short adsorption time.

As shown in Fig. 3, the zeta potential of the Fe_3O_4 was always negative, similar to the study by Toh et al. [15]. When Fe_3O_4 particles were dissolved in water, the bare Fe and O on the particle surface would quickly combine with water,

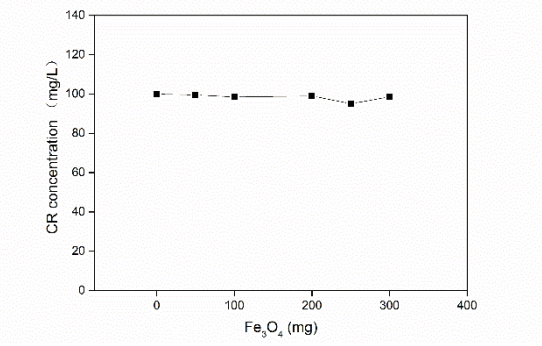

Fig. 2. Effect of Fe_3O_4 doses on CR adsorption.

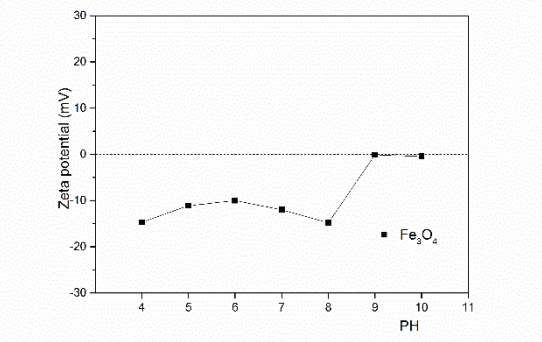

Fig. 3. Zeta potential of Fe_3O_4 as a function of pH.

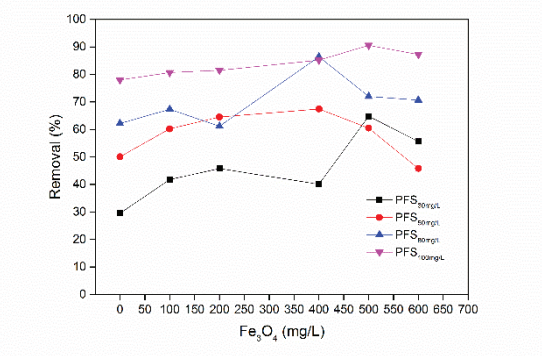

Fig. 4. Effect of Fe_3O_4 on removal value of CR.

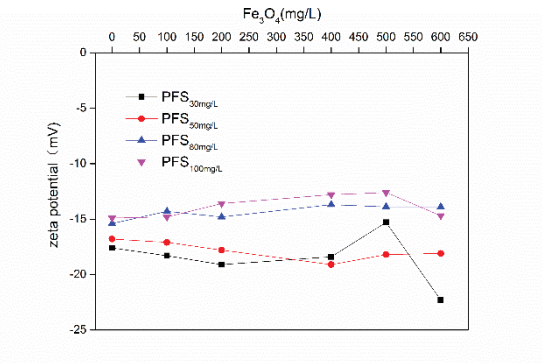

Fig. 5. Effect of Fe_3O_4 on the zeta potentials of the supernatants after flocculation.

and adsorb OH^-or H^+ ions to form Fe–OH, which brought a negative charge [15]. However, there are also studies that have shown that Fe_3O_4 particles are amphoteric. When it was dissolved in water, it would quickly combine with water and form Fe–OH, and the Fe–OH on the surface could produce positively charged Fe–OH^{2+} and negatively charged Fe–O^- by the protonation and deprotonation reactions. In this situation, it was positively charged below the isoelectric point and negatively charged above the isoelectric point [29]. It may be due to the different properties of the Fe_3O_4 particles synthesized by different methods.

3.2. Flocculation experiments

The flocculation experiments of CR were carried out under pH of 7.80, which was the average pH value of tap water. The removal values with different dosage were shown in Fig. 4.

It can be seen from Fig. 4 that PFS–Fe_3O_4 had improved the removal value within the dosage range investigated. The CR removal curves associated with different dosages of Fe_3O_4 exhibited similar changing trends with the increase of Fe_3O_4: slow increase at low dosage, then followed by a rapid increase with high dosage. However, it decreased when the concentration was greater than a certain value. At PFS dosage of 30 mg/L, the removal rate increased from 29.5% to 64.8% with the addition of 500 mg/L Fe_3O_4. While the removal value of 80 mg/L PFS can only reach 62.20%, the effect of Fe_3O_4 for the coagulation was quite significant. However, when the concentration of Fe_3O_4 reached 600 mg/L, the removal rate tended to decrease. The zeta potential as a function of Fe_3O_4 dosage is shown in Fig. 5. With the increase of the concentration of Fe_3O_4 particles, the zeta potential had a small increase. However, it can be seen that the zeta potential of the flocculated supernatant did not change much, so its enhancement of the neutralization ability was limited. It indicated that the mechanism of removing CR was different from that of algae and the humic acid–kaolin system [30].

In previous studies [31], the PFS itself contains a large amount of polynuclear complex ions, such as $Fe_3(OH)_4^{5+}$, $Fe_6(OH)_{12}^{6+}$, and $Fe_4O(OH)_4^{6+}$, which were formed by OH bridges and large number of inorganic macromolecular compounds with positive charges [14]. The principle mechanism for the coagulation by PFS is adsorbing-bridging and may follow sweep coagulation [32], which was in accordance with the changes of the zeta potential associated with different dosages of PFS. CR is an anionic dye, which could be involved in a dual mechanism including coagulation by charge neutralization and flocculation by bridging mechanism. The Fe_3O_4 have relatively large specific surface areas, which easily lead the single-molecule aggregates to multi-molecule aggregates. When PFS and Fe_3O_4 were combined to flocculate CR, one end or segment of the PFS would react with Fe_3O_4 by ion exchange and formed the sun-like structure. According to the relevant research [14], the hydroxyl groups on the surface of Fe_3O_4 can react with PFS by ion exchange, that is, $–Fe_n–(OH)_m$ group from PFS displaces H^+ ions from hydroxyl to form the structure $–Fe–O–Fe_n(OH)_m$.

The concentration of Fe_3O_4–PFS increased with the increase of Fe_3O_4. The sun-like structured Fe_3O_4–PFS reacted with CR immediately after dosed. Because only one end or segment of PFS chains attached to the CR in the flocs, and only a portion of the positive charge on PFS chains can neutralize the negative charge of the CR. Although the charge neutralization ability of PFS was weakened, the sun-like structure of the flocs produced by Fe_3O_4–PFS contributed the effect of adsorbing-bridging. Thus, the removal rate was improved.

However, it was also noted that with the increase of the concentration of Fe_3O_4, the removal rate of the Fe_3O_4–PFS decreased locally and then increased. This may be due to the inadequate stirring process of the Fe_3O_4 and the PFS or a few other factors.

In the experiment of investigating the influence of the Fe_3O_4 on the removal of the dye, the magnetic field was not

applied. However, in the experiment of removing algae, the heavy metal or the humic acid–kaolin system, the improved results only showed under magnetic field. This can only be caused by some other unknown factors related to the properties of CR.

3.3. The effect of pH on the flocculation performance

The coagulation–flocculation performance and the effect of pH on the removal of CR were comparatively investigated in this study. The removal value of PFS and Fe_3O_4–PFS in treating CR is shown in Fig. 6. The curves associated with the two coagulants exhibited similar changing trends: when the pH was less than 6, the removal value was close to 100%, forming relatively larger flocs, with the increase of pH, removal rate gradually decreased. CR contains a sulfonic acid group and an amino group. When it was dissolved in water, it was negatively charged. The electrostatic repulsion between negative charges on different molecules enhanced the solubility of dyes. As the pH gradually decreased, the protonation processes of the dye reduced its charge density and induced self-aggregation of the dye molecules. Therefore, less coagulant would be required to destabilize it under acidic conditions, and more coagulants were needed in alkaline and neutral environment [33]. However, when the pH reached 8, the adsorbing-bridging effect of PFS was enhanced, thus the removal value was improved. It was noted that PFS gave poor removal results than Fe_3O_4–PFS within the dosage range investigated, and flocs produced by Fe_3O_4–PFS precipitated more rapidly even in the absence of external magnetic field. Fe_3O_4–PFS performed always better than PFS at any pH, and especially at pH = 7 or 8, the removal rate is increased by about 13%. The efficiency of coagulation–flocculation not only depends on the solubility and chemical structures of dyes but also the characteristics of the coagulants–flocculants. So, it can be concluded that Fe_3O_4–PFS works extremely better in near-neutral environments.

The polymerization of ferric sulfate hydrolysis process can be seen from Fig. 7. In the acidic environment, mainly free ions and mononuclear hydroxyl complexes exist (Fe_a), with the increase of pH, gradually into a transitional polymer state (Fe_b), and finally into precipitated species (Fe_c) [32]. As mentioned in Section 3.2, Fe–O–$Fe_n(OH)_m$ was formed on the surface of Fe_3O_4 particles. When pH = 7 or so, Fe_b was the majority species [7]. At this time, the Fe_b easily covered the surface of the Fe_3O_4 particles and formed the sun-like structure with the Fe_3O_4 particles as the skeleton. The structure of the composite coagulants enhanced the adsorbing-bridging effect. In addition, the addition of Fe_3O_4 affected the balance of H^+ and OH^-, driving the balance to the right and promoting the formation of Fe_b to further enhance the flocculation effect [17].

In addition to these, the formation of a floc with Fe_3O_4 increased the weight of the flocs and thus allowed the floc to precipitate more rapidly. Therefore, PFS–Fe_3O_4 works at a broader range even in the absence of external magnetic field.

3.4. The dosing strategy

There were three dosing strategies. The structures of the three different flocs are shown in Fig. 8. The first was that PFS was dosed first followed by Fe_3O_4 (expressed as PFS+Fe_3O_4), that is, PFS and CR were first combined, and then the PFS–CR interacted with the Fe_3O_4. The second was to add Fe_3O_4 first and then followed by PFS (expressed as Fe_3O_4+PFS), this time, after Fe_3O_4 was added, it can be quickly mixed with CR and thus form a mixed system of CR–Fe_3O_4. The PFS added later can bridge PFS and Fe_3O_4. The third one was to add Fe_3O_4 and PFS at the same time (expressed as Fe_3O_4–PFS). In this condition, the surface of bare magnetic Fe_3O_4 nanoparticles was firstly combined with PFS and then contacted CR.

As we can see in Fig. 9, when 200 mg/L Fe_3O_4 was added, Fe_3O_4–PFS removal rate increased by 14.43%, while the PFS+Fe_3O_4 and Fe_3O_4+PFS increased by 2.81% and 8.01%, respectively. When the Fe_3O_4 was added at 400 mg/L, the removal value of Fe_3O_4–PFS increased by 17.37%, and PFS+Fe_3O_4 and Fe_3O_4+PFS increased by 4.31% and 9.61%, respectively.

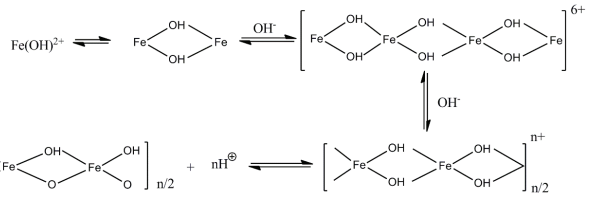

Fig. 7. Simplified scheme of the hydrolysis–polymerization process of PFS.

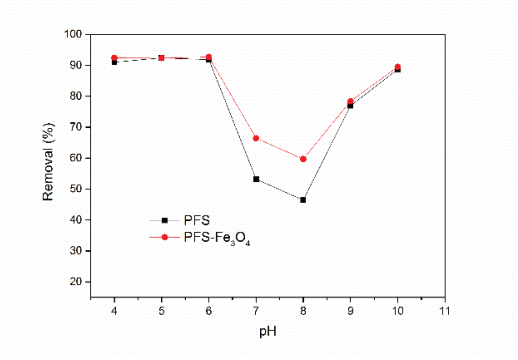

Fig. 6. Removal of CR by coagulation as a function of pH and coagulant dosage.

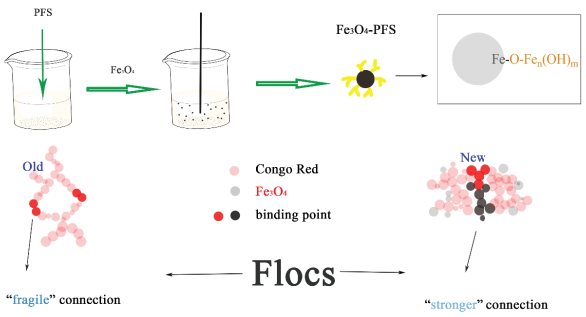

Fig. 8. The possible flocculation mechanism of the flocculant.

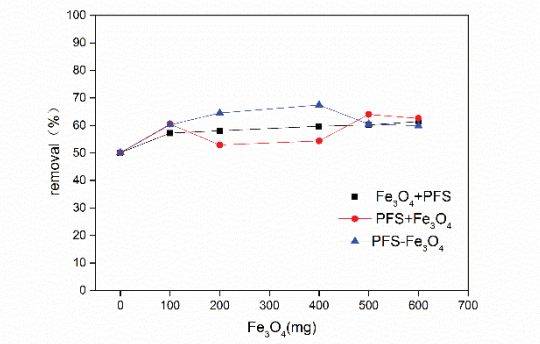

Fig. 9. Effect of different dosage strategy on removal value of CR.

The results of Fe_3O_4–PFS were obviously superior to that of PFS+Fe_3O_4 and Fe_3O_4+PFS from 200 to 400 mg/L. These differences showed that the increased number of particles was not the dominants mechanism, which was different from the conclusion of Prochazkova et al. [14] dealing with CMP wastewater. It could be seen that the performance of Fe_3O_4+PFS is better than PFS+Fe_3O_4. The order of color removal was Fe_3O_4–PFS > Fe_3O_4+PFS > PFS+Fe_3O_4.

According to Fig. 5, the adsorbing-bridging was the main mechanism. So, the presence of Fe_3O_4 contributes to the effect of adsorbing-bridging.

In addition, the Fe_3O_4–PFS was black and well distributed. PFS was chelated and adsorbed on the surface of bare Fe_3O_4, which enhanced the stability of colloidal particles and could fully disperse in CR solution [34]. However, Fe_3O_4+PFS did not show obviously black, and PFS+ Fe_3O_4 was slightly black. Fe_3O_4+PFS and Fe_3O_4+PFS tended to agglomerate and precipitate under the Van der Waals force, magnetic attraction, and gravity, and could not form a stable suspension system, thus reducing the chance of Fe_3O_4 to bind with CR and PFS, finally, the removal rate was decreased. In the other situation, for PFS+Fe_3O_4, after PFS was added, PFS quickly combined with the CR. With the addition of Fe_3O_4, the Fe_3O_4 would be combined with some flocs, not easy to directly precipitate and therefore the solution was pan-black. For Fe_3O_4+PFS, most of the Fe_3O_4 tended to precipitate to the bottom, only a small part of the Fe_3O_4 stay in the solution, so no obviously black was observed. However, Fe_3O_4+PFS showed better performance than PFS+Fe_3O_4, it further demonstrated that the structure of the flocs played an important role.

When the dosage of Fe_3O_4 is less than 100 mg/L or more than 500 mg/L, the three kinds of dosing methods showed almost the same performance. When a small amount of Fe_3O_4 was added, the structure of the flocs did not show much difference. When the amount of Fe_3O_4 dosing is large, a part of the Fe_3O_4 directly sinks to the bottom of the beaker, and the other part enhances the combination of PFS and Fe_3O_4, finally resulting in similar removal value of the three dosing methods at this time.

3.5. Floc morphological characteristics

It can be seen from Fig. 10 that the Fe_3O_4 dispersed around the flocs and in the agglomeration state. The following structures were observed under careful observation: (1) the floc adhered to the periphery of the Fe_3O_4, (2) the Fe_3O_4 sandwiched Congo Red floc body, and (3) Congo Red flocs sedimented alone. Among them, the first structure is of the majority. As can be seen from Fig. 11, Fe_3O_4 gathered in different sizes with uneven distribution. With the larger specific surface area of Fe_3O_4, the flocs can adhere to the periphery of the Fe_3O_4, thus larger flocs were formed. Finally, an improved removal value was gotten.

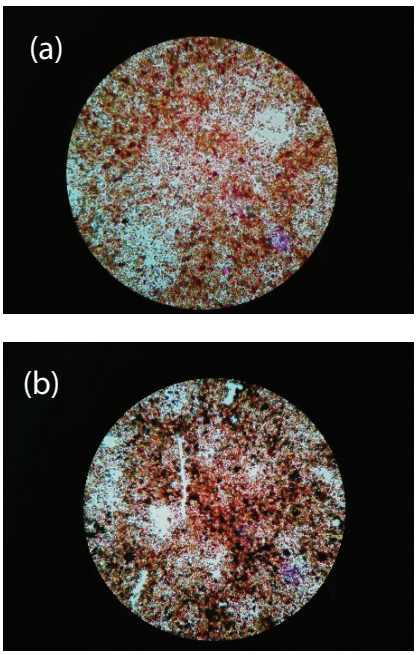

Fig. 10. Flocs under the optical microscope (×100) after magnetic flocculation: (a) the flocs flocculate by PFS and (b) the flocs flocculate by Fe_3O_4–PFS.

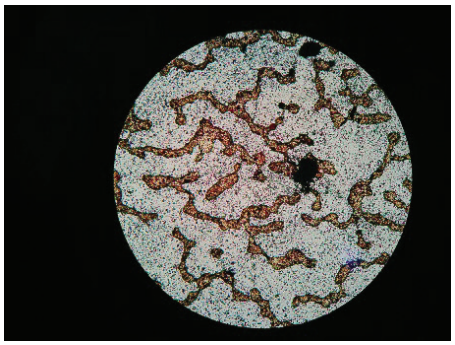

Fig. 11. Flocs under the optical microscope (×400) after magnetic flocculation by Fe_3O_4–PFS.

As we can see from Fig. 4, the removal value decreased with excessive Fe_3O_4. With the increase of the Fe_3O_4, the part of the magnetic skeleton would increase which resulted in the rapid precipitation. In return, the removal value decreased.

3.6. Characteristics

In order to further demonstrate the structure of the flocs, the FTIR spectra of flocculants and flocs are shown in Fig. 12. Floc1 was produced by PFS and floc2 was produced by Fe_3O_4–PFS. Broad peaks at 3,500–3,200 cm^{-1} and 1,612–1,635 cm^{-1} were observed for all the samples and

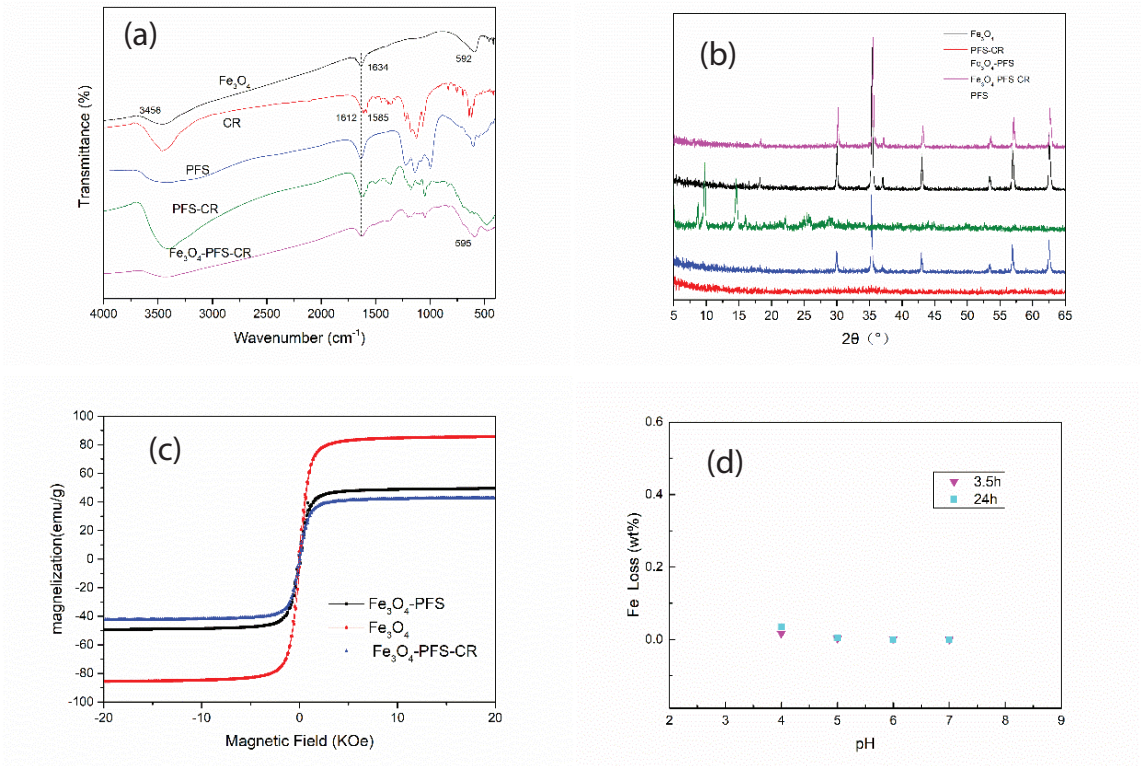

Fig. 12. Characterization results of (a) FTIR spectra, (b) XRD patterns, (c) magnetic hysteresis curve, and (d) leaching of Fe from flocculants at different pH levels.

Table 1
The characteristics of PFS–CR and Fe_3O_4–PFS–CR

Flocs	D_f	R^2	d(0.1)	d(0.5)	d(0.9)
PFS–CR	1.23	0.96	5.832	13.300	45.797
Fe_3O_4–PFS–CR	1.75	0.97	16.707	32.793	59.100

corresponded to the stretching vibration of –OH and to the vibration of water absorbed, or complexed in the coagulant [35]. PFS contained a large amount of sulfate, so the peak appeared at 998–1,224 cm^{-1} was the vibration of S=O or/and O=S=O [31]. Fe_3O_4 appeared relatively strong absorption peak at 592 cm^{-1}, which was due to the vibration of Fe–O group [35]. In the spectrum of CR, the peak at 1,322–1,500 cm^{-1} and 419–920 cm^{-1} attributed to the vibration of benzene ring and its substituent, the absorption peak at 1,066–1,226 cm^{-1} was due to the presence of SO_4^{2-} group.

Compared with the spectrum of the two flocs, we could see that both of the two flocs have obvious benzene ring and its substituted hydrocarbon absorption peak, indicating the existence of CR. For floc2, a broad peak at 596 cm^{-1}, which was found in the spectrum of Fe_3O_4 but not in the spectrum of floc1, was contributed to the vibration of Fe–O group. All of these indicated that the structure of Fe_3O_4–PFS–CR was formed.

The powder XRD patterns in Fig. 12(b) exhibit that magnetite particles are found in Fe_3O_4, Fe_3O_4–PFS, and Fe_3O_4–PFS–CR as the diffraction peaks at 30.2°, 35.5°, 43.1°, 53.4°, 57.0°, and 63.1°are assigned to the cubic spinel structure of Fe_3O_4, indicating that the coating process did not

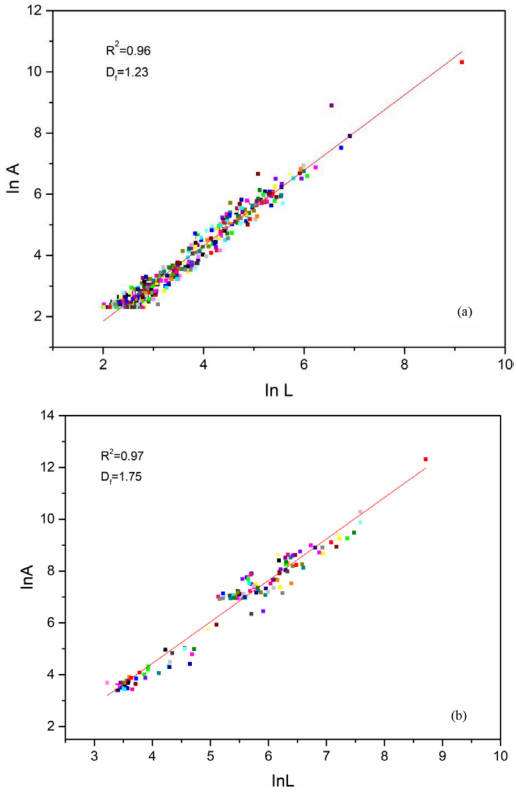

Fig. 13. Fractal dimension and correlation coefficients: (a) PFS–CR and (b) Fe_3O_4–PFS–CR.

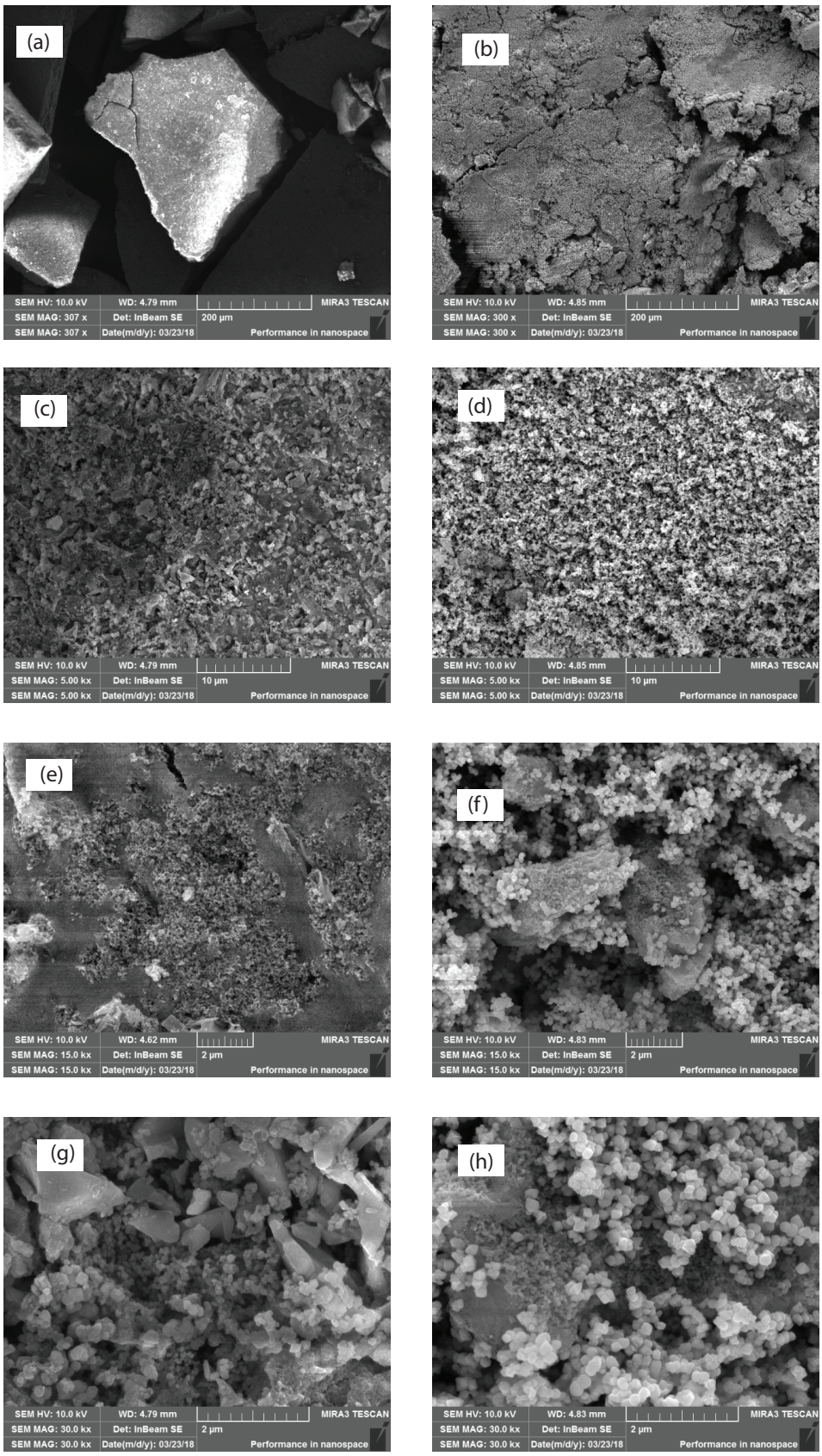

Fig. 14. SEM images of various samples: (a) PFS-flocs (×300), (b) Fe_3O_4–PFS-flocs (×300), (c) PFS-flocs (×5,000), (d)Fe_3O_4–PFS-flocs (×5,000), (e) PFS-flocs (×15,000), (f) Fe_3O_4–PFS-flocs (×15,000), (g) PFS-flocs (×30,000), (h) Fe_3O_4–PFS-flocs (×30,000).

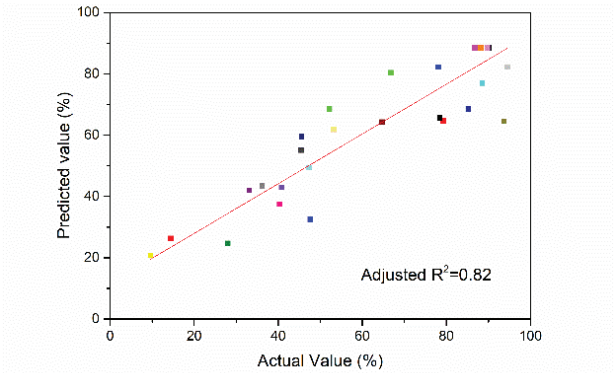

Fig. 15. Parity plot for the experimental and predicted values of removal value of the dye.

induce any phase change of Fe_3O_4 and further demonstrates the successful combination of flocs. After coating, the intensities of corresponding diffraction peaks for magnetic flocculants were significantly reduced because of the layer of PFS or PFS–CR on the particle surface. The hysteresis loop of each curve in Fig. 12(c) demonstrated superparamagnetic properties. The saturation magnetization values (M_s) were measured to be 85.60, 49.35, and 42.64 emu g^{-1}, respectively, for Fe_3O_4, Fe_3O_4–PFS, and Fe_3O_4–PFS–CR. Obviously, the M_s value decreased after coating, but the relatively high saturation magnetization significantly facilitates separation and regeneration of it.

Taking into account the economic costs of water treatment, the stability of Fe_3O_4 was investigated to evaluate its application potential in removal of organic dyes. As can

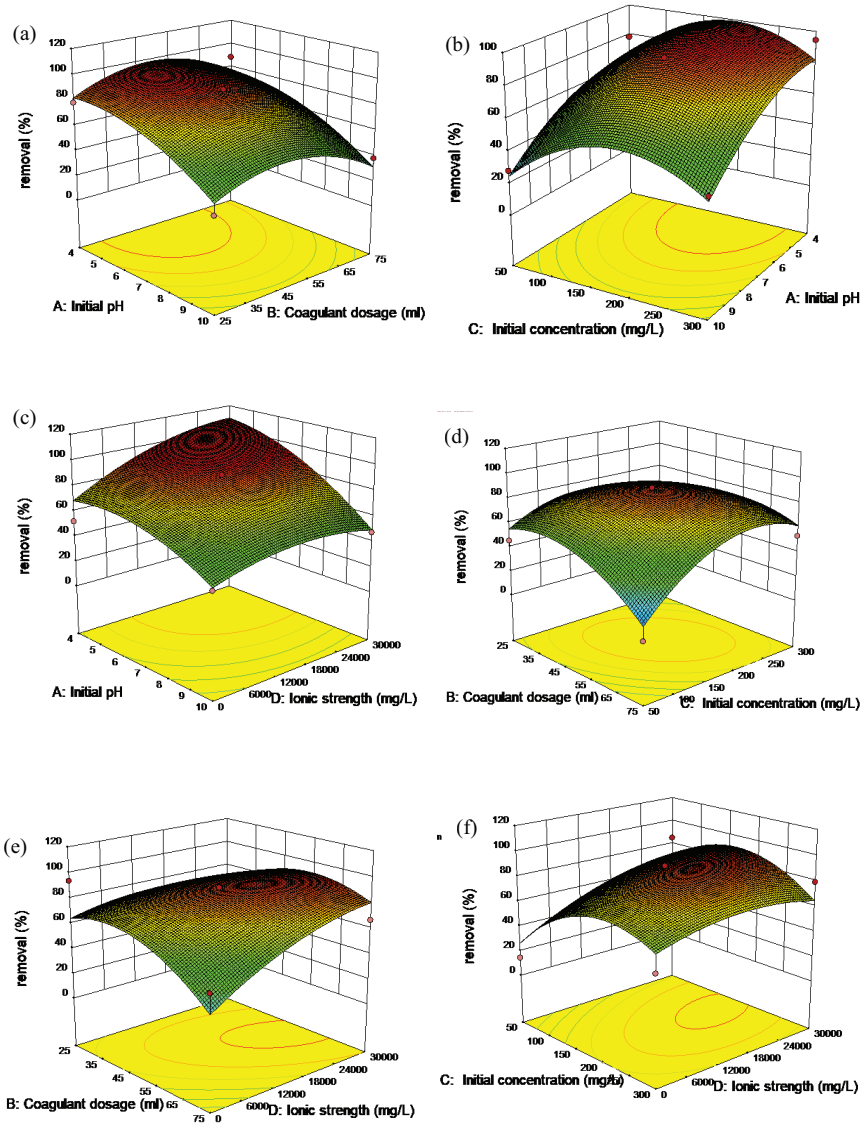

Fig. 16. Coagulation–flocculation optimization using RSM–BBD: (a) surface plots for removal value of the dye: initial pH and coagulant dosage (initial concentration = 175 mg/L, ionic strength = 15,000 mg/L), (b) initial pH and initial concentration (coagulant dosage = 50 mL, ionic strength = 15,000 mg/L) at pH 7, (c) initial pH and ionic strength (coagulant dosage = 50 mL, initial concentration = 175 mg/L), (d) coagulant dosage and initial concentration (initial pH = 7, ionic strength = 15,000 mg/L), (e) coagulant dosage and ionic strength (initial pH = 7, initial concentration = 175 mg/L), (f) initial concentration and ionic strength (initial pH = 7, coagulant dosage = 50 mL).

be seen from the analysis of pH dependence in Fig. 12(d), the leaching rate at the pH studied was very low, implying that leaching of Fe was ignorable.

3.7. Characteristics of flocs

To demonstrate the structure of flocs, characteristics of flocs by PFS flocculation and Fe_3O_4–PFS flocculation were compared in this study. Fractal dimension and particle size distribution are displayed in Table 1 and Fig. 13, revealing the difference between the two kinds of flocs. Table 1 illustrates that fractal dimension and the particle size of Fe_3O_4–PFS–CR were higher than PFS–CR, which revealed that the structure of Fe_3O_4–PFS–CR were denser and compacter than that of PFS–CR. When the PFS was used to flocculate CR, the charge neutralization was the dominated mechanism. The force of electrostatic and Van der Waals were weak, so loosely PFS–CR were formed.

The morphology of the flocs in the absence and presence of Fe_3O_4 exhibited in Fig. 14 provided further structure evidence of the flocculation mechanism. The SEM pictures revealed that the flocs, of small size and randomly separated, in the absence of the Fe_3O_4 are gathered in bigger aggregates after the formation of the flocs based on Fe_3O_4. In addition, PFS–CR had relative regular structure and smooth surface in Fig. 14(a). However, Fe_3O_4–PFS–CR possessed tiny and sharp bulges on the surface and formed loose condensed structure based on the rigid skeleton of Fe_3O_4. Fe_3O_4–PFS–CR combined Fe_3O_4 and PFS, and flexible branches and rigid structures penetrate each other. The embedded structure added the surface area to interact with each other, and thus the ability of adsorbing was enhanced. In addition, the weight of the flocs was heavier which was conducive for forming denser and compacter flocs. What more is that the porous morphologies of samples can improve the ability to adsorbing and flocculating purities in water. Finally, a better result was gotten.

3.8. Optimization of coagulation–flocculation using RSM–BBD

The experimental design matrix used for the coagulation–flocculation optimization together with the experimental and predicted residual turbidities is listed in Table S2. According to the experimental results, the best second-order polynomial equation was obtained as follows:

$$\begin{aligned} Y = {} & -52.68 + 15.08X_1 + 1.76X_2 + 0.49X_3 + 0.00264X_4 - 0.018X_1X_2 \\ & - 0.00251X_1X_3 - 0.000193X_1X_4 + 0.00422X_2X_3 + 0.000032X_2X_4 \\ & - 0.00000494X_3X_4 - 1.29X_1^2 - 0.03X_2^2 - 0.00156X_3^2 - 0.0000000414X_4^2 \end{aligned} \quad (3)$$

For a reliable model, the predicted data of the residual turbidity should be compared with the experimental data. Fig. 15 shows that the experimental data agree well with the predicted data of the removal value. The adjusted R^2 value of 0.82 suggested the fitness of the model, because magnetic coagulation is always instability. Furthermore, the adequacy of the model was justified through analysis of variance (ANOVA) as shown in Table S3. The values of 'Prob > *F*' less than 0.0500 indicated that the model terms were significant as indicated in Table S3.

The response surface 3D plots for a better explanation for the independent variables and their interactive effects on the removal value of the dye are presented in Fig. 16. Here, the pH value and ionic strength played a key role in the coagulation–flocculation process. pH and ionic strength can greatly influence the property of PFS, thus the performance of PFS–Fe_3O_4 was changed.

It can be concluded that the performance of PFS–Fe_3O_4 mainly depended on the property of PFS. The denser and compacter flocs of PFS–Fe_3O_4 induced the higher removal value.

4. Conclusion

This paper presents a new method to remove soluble anion dye, Congo Red. In this method, the Fe_3O_4 was combined with the PFS to remove the CR without external magnetic field for the first time. This study shows that pH, the ratio of Fe_3O_4 and PFS, and the method of dosing have a great impact on the effect of magnetic coagulation–flocculation. After PFS was dissolved in water, polynuclear complex ions were formed by OH bridges. The polynuclear complex ions had a very large surface area and were positively charged, with the addition of Fe_3O_4, the sun-like structure of Fe–O–$Fe_n(OH)_m$ was formed. As shown in Fig. 8, when PFS–Fe_3O_4 was added to the Congo Red solution, the denser, compacter, and larger flocs were formed, which strengthened the effect of adsorbing-bridging, and thus the removal value was improved. The method breaks the limit to remove the soluble dyes by magnetic coagulation and enriches the theoretical research foundation of magnetic coagulation that is of guiding significance for the expansion of this field. By using the method, the flocs produced by magnetic coagulation can rapidly remove the flocs under the condition of applied magnetic field, which can significantly reduce the settling time. In addition, the dosage of inorganic flocculants needed significantly decreased. The used Fe_3O_4 is environmentally friendly, has no secondary pollution, and is easy to be recovered. Therefore, the method has the advantages of high efficiency, simplicity, no secondary pollution, and has a wide range of applications.

Acknowledgment

The authors are grateful for the financial support provided by the National Natural Science Foundation of China (project nos.: 21677020 and 21477010).

References

[1] O.G. Apul, T. Karanfil, Adsorption of synthetic organic contaminants by carbon nanotubes: a critical review, Water Res., 68 (2015) 34–55.
[2] S.M.R. Shaikh, M.S. Nasser, I. Hussein, A. Benamor, S.A. Onaizi, H. Qiblawey, Influence of polyelectrolytes and other polymer complexes on the flocculation and rheological behaviors of clay minerals: a comprehensive review, Sep. Purif. Technol., 187 (2017) 137–161.
[3] I. Levchuk, J.J. Rueda Márquez, M. Sillanpää, Removal of natural organic matter (nom) from water by ion exchange – a review, Chemosphere, 192 (2017) 90–104.
[4] G. Boczkaj, A. Fernandes, Wastewater treatment by means of advanced oxidation processes at basic pH conditions: a review, Chem. Eng. J., 320 (2017) 608–633.

[5] X. Li, Y. Mo, J. Li, W. Guo, H.H. Ngo, In-situ monitoring techniques for membrane fouling and local filtration characteristics in hollow fiber membrane processes: a critical review, J. Membr. Sci., 528 (2017) 187–200.
[6] J. Park, N. Yamashita, C. Park, T. Shimono, D.M. Takeuchi, H. Tanaka, Removal characteristics of pharmaceuticals and personal care products: comparison between membrane bioreactor and various biological treatment processes., Chemosphere, 179 (2017) 347.
[7] J. Duan, J. Gregory, Coagulation by hydrolysing metal salts, Adv. Colloid Interface Sci., 100–102 (2003) 475–502.
[8] S.L. Chai, J. Robinson, F.C. Mei, A review on application of flocculants in wastewater treatment, Process Saf. Environ. Prot., 92 (2014) 489–508.
[9] F. Renault, B. Sancey, P.M. Badot, G. Crini, Chitosan for coagulation/flocculation processes – an eco-friendly approach, Eur. Polym. J., 45 (2009) 1337–1348.
[10] J. Beltránheredia, J. Sánchezmartín, Municipal wastewater treatment by modified tannin flocculant agent, Desalination, 249 (2009) 353–358.
[11] L.G. Torres, S.L. Carpinteyrourban, Use of *Prosopis laevigata* seed gum and *Opuntia ficus-indica* mucilage for the treatment of municipal wastewaters by coagulation–flocculation, Nat. Resour. J., 3 (2012) 35–41.
[12] T. Tripathy, R.P. Singh, Characterization of polyacrylamide-grafted sodium alginate: a novel polymeric flocculant, J. Appl. Polym. Sci., 81 (2001) 3296–3308.
[13] K.H. Kan, J. Li, K. Wijesekera, E.D. Cranston, Polymer-grafted cellulose nanocrystals as pH-responsive reversible flocculants., Biomacromolecules, 14 (2013) 3130–3139.
[14] G. Prochazkova, N. Podolova, I. Safarik, V. Zachleder, T. Branyik, Physicochemical approach to freshwater microalgae harvesting with magnetic particles, Colloids Surf., B, 112 (2013) 213–218.
[15] P.Y. Toh, B.W. Ng, C.H. Chong, A.L. Ahmad, J.W. Yang, J.C.D. Chan, J.K. Lim, Magnetophoretic separation of microalgae: the role of nanoparticles and polymer binder in harvesting biofuel, RSC Adv., 4 (2013) 4114–4121.
[16] L. Xu, C. Guo, F. Wang, S. Zheng, C.Z. Liu, A simple and rapid harvesting method for microalgae by in situ magnetic separation, Bioresour. Technol., 102 (2011) 10047–10051.
[17] K. Lee, S.Y. Lee, J.G. Na, G.J. Sang, R. Praveenkumar, D.M. Kim, W.S. Chang, Y.K. Oh, Magnetophoretic harvesting of oleaginous *Chlorella* sp. by using biocompatible chitosan/magnetic nanoparticle composites, Bioresour. Technol., 149 (2013) 575–578.
[18] Y. Chen, L. Man, W. Cai, Influence of operating parameters on the performance of magnetic seeding flocculation, Environ. Sci. Pollut. Res., 23 (2016) 1–9.
[19] K. Mandel, F. Hutter, C. Gellermann, G. Sextl, Modified superparamagnetic nanocomposite microparticles for highly selective Hg(II) or Cu(II) separation and recovery from aqueous solutions, ACS Appl. Mater. Interfaces, 4 (2012) 5633–5642.
[20] C.J. Chin, P.W. Chen, L.J. Wang, Removal of nanoparticles from CMP wastewater by magnetic seeding aggregation, Chemosphere, 63 (2006) 1809–1813.
[21] Y. Zhao, W. Liang, L. Liu, F. Li, Q. Fan, X. Sun, Harvesting *Chlorella vulgaris* by magnetic flocculation using Fe_3O_4 coating with polyaluminium chloride and polyacrylamide, Bioresour. Technol., 198 (2015) 789.
[22] D. Liu, P. Wang, G. Wei, W. Dong, F. Hui, Removal of algal blooms from freshwater by the coagulation-magnetic separation method, Environ. Sci. Pollut. Res., 20 (2013) 60–65.
[23] C. Jiang, R. Wang, W. Ma, The effect of magnetic nanoparticles on *Microcystis aeruginosa* removal by a composite coagulant, Colloids Surf., A, 369 (2010) 260–267.
[24] Y. Li, J. Wang, Y. Zhao, Z. Luan, Research on magnetic seeding flocculation for arsenic removal by superconducting magnetic separation, Sep. Purif. Technol., 73 (2010) 264–270.
[25] P. Anand, J. Etzel, F. Friedlaender, Heavy metals removal by high gradient magnetic separation, IEEE Trans. Magn., 21 (1985) 2062–2064.
[26] W. Zhang, Z. Chen, B. Cao, Y. Du, C. Wang, D. Wang, T. Ma, H. Xia, Improvement of wastewater sludge dewatering performance using titanium salt coagulants (TSCS) in combination with magnetic nano-particles: significance of titanium speciation, Water Res., 110 (2016) 102–111.
[27] N. Gokon, A. Shimada, N. Hasegawa, H. Kaneko, M. Kitamura, Y. Tamaura, Ferrimagnetic coagulation process for phosphate ion removal using high-gradient magnetic separation, Sep. Purif. Technol., 37 (2002) 3781–3791.
[28] R.K. Chakraborti, J.F.A. And, J.E.V. Benschoten, Characterization of alum floc by image analysis, Environ. Sci. Technol., 34 (2000) 3969–3976.
[29] A. Hajdú, E. Illés, E. Tombácz, I. Borbáth, Surface charging, polyanionic coating and colloid stability of magnetite nanoparticles, Colloids Surf., A, 347 (2009) 104–108.
[30] M. Zhang, F. Xiao, D. Wang, X. Xu, Q. Zhou, Comparison of novel magnetic polyaluminum chlorides involved coagulation with traditional magnetic seeding coagulation: coagulant characteristics, treating effects, magnetic sedimentation efficiency and floc properties, Sep. Purif. Technol., 182 (2017) 118–127.
[31] A.I. Zouboulis, P.A. Moussas, F. Vasilakou, Polyferric sulphate: preparation, characterisation and application in coagulation experiments, J. Hazard. Mater., 155 (2008) 459.
[32] A.K. Verma, R.R. Dash, P. Bhunia, A review on chemical coagulation/flocculation technologies for removal of colour from textile wastewaters, J. Environ. Manage., 93 (2012) 154–168.
[33] B. Shi, G. Li, D. Wang, C. Feng, H. Tang, Removal of direct dyes by coagulation: the performance of preformed polymeric aluminum species, J. Hazard. Mater., 143 (2007) 567–574.
[34] S.C. Tang, I.M. Lo, Magnetic nanoparticles: essential factors for sustainable environmental applications, Water Res., 47 (2013) 2613–2632.
[35] D. Akin, A. Yakar, U. Gündüz, Synthesis of magnetic Fe_3O_4-chitosan nanoparticles by ionic gelation and their dye removal ability, Water Environ. Res., 87 (2015) 425.

Supplementary material

Table S1
Levels and codes of Box–Behnken design

Factor	Codes		Level	
	x_1	–1	0	1
Initial pH	X_1	4	7	10
Coagulant dosage/mL	X_2	25	50	75
Initial concentration	X_3	50	175	300
Ionic strength	X_4	0	15,000	30,000

Table S2
Box–Behnken experiment plan and result

Experiment number	Codes				Actual				Removal percentage	
	x_1	x_2	x_3	x_4	X_1	X_2	X_3	X_4	Actual	Predicted
1	0	0	0	0	7	50	175	15,000	90.11	88.49
2	0	0	1	1	7	50	300	30,000	79.30	64.73
3	–1	0	0	–1	4	50	175	0	52.17	68.50
4	–1	–1	0	0	4	25	175	15,000	78.11	82.18
5	0	0	0	0	7	50	175	15,000	87.60	88.49
6	0	0	0	0	7	50	175	15,000	86.74	88.49
7	0	1	–1	0	7	75	50	15,000	9.60	20.76
8	0	–1	0	–1	7	25	175	0	93.71	64.49
9	0	0	1	–1	7	50	300	0	45.53	59.47
10	1	–1	0	0	10	25	175	15,000	33.14	41.99
11	0	–1	0	1	7	25	175	30,000	64.74	64.21
12	1	0	–1	0	10	50	50	15,000	28.00	24.65
13	–1	0	0	1	4	50	175	30,000	93.49	109.64
14	0	0	–1	1	7	50	50	30,000	85.20	68.56
15	0	0	0	0	7	50	175	15,000	88.23	88.49
16	1	0	0	–1	10	50	175	0	40.80	42.97
17	1	0	1	0	10	50	300	15,000	40.33	37.44
18	1	1	0	0	10	75	175	15,000	38.11	31.35
19	–1	0	1	0	4	50	300	15,000	94.50	82.23
20	0	–1	1	0	7	25	300	15,000	36.20	43.36
21	0	1	1	0	7	75	300	15,000	53.20	61.84
22	1	0	0	1	10	50	175	30,000	47.37	49.37
23	0	0	0	0	7	50	175	15,000	89.77	88.49
24	0	–1	–1	0	7	25	50	15,000	45.40	55.09
25	–1	0	–1	0	4	50	50	15,000	78.40	65.67
26	0	0	–1	–1	7	50	50	0	14.40	26.28
27	0	1	0	1	7	75	175	30,000	66.74	80.34
28	0	1	0	–1	7	75	175	0	47.60	32.51
29	–1	1	0	0	4	75	175	15,000	88.51	76.97

Table S3
ANOVA test for the residual turbidity of the surfactant effluent

Term	Sum of squares	Degree of freedom	Mean square	*F*-value	*P*-value	Remarks
Model	15,380.9	14	1,098.6	4.3	0.0051	Significant
X_1	5,522.3	1	5,522.3	21.6	0.0004	Significant
X_2	188.4	1	188.4	0.7	0.4056	Insignificant
X_3	646.3	1	646.3	2.5	0.1345	Insignificant
X_4	1,695.1	1	1,695.1	6.6	0.0221	Significant
X_1X_2	7.4	1	7.4	0.0	0.8678	Insignificant
X_1X_3	3.5	1	3.5	0.0	0.9080	Insignificant
X_1X_4	301.8	1	301.8	1.2	0.2961	Insignificant
X_2X_3	697.0	1	697.0	2.7	0.1213	Insignificant
X_2X_4	578.7	1	578.7	2.3	0.1550	Insignificant
X_3X_4	342.9	1	342.9	1.3	0.2667	Insignificant
X_1^2	868.1	1	868.1	3.4	0.0869	
X_2^2	2,292.8	1	2,292.8	9.0	0.0097	Significant
X_3^2	3,870.8	1	3,870.8	15.1	0.0016	Significant
X_4^2	561.5	1	561.5	2.2	0.1609	Insignificant
Residual	3,586.3	14	256.2			
Lack of fit	3,578.1	10	357.8	174.7	<0.0001	Significant
Pure error	8.2	4	2.0			
Correction total	18,967.2	28				